ACS APPLIED MATERIALS & INTERFACES

Research Article

Cite This: ACS Appl. Mater. Interfaces 2018, 10, 19019−19026

www.acsami.org

Novel Series of Quasi-2D Ruddlesden−Popper Perovskites Based on Short-Chained Spacer Cation for Enhanced Photodetection

Ruoting Dong,[†] Changyong Lan,[†,∥] Xiuwen Xu,[†] Xiaoguang Liang,[†,⊥] Xiaoying Hu,[∥] Dapan Li,[†,⊥] Ziyao Zhou,[†,⊥] Lei Shu,[†,‡,⊥] SenPo Yip,[†,‡,⊥] Chun Li,[∥] Sai-Wing Tsang,[†] and Johnny C. Ho*[,†,‡,§,⊥]

[†]Department of Materials Science and Engineering, [‡]State Key Laboratory of Millimeter Waves, and [§]Centre for Functional Photonics, City University of Hong Kong, Kowloon 999077, Hong Kong

[∥]School of Optoelectronic Science and Engineering, University of Electronic Science and Technology of China, Chengdu 610054, P. R. China

[⊥]Shenzhen Research Institute, City University of Hong Kong, Shenzhen 518057, P. R. China

Supporting Information

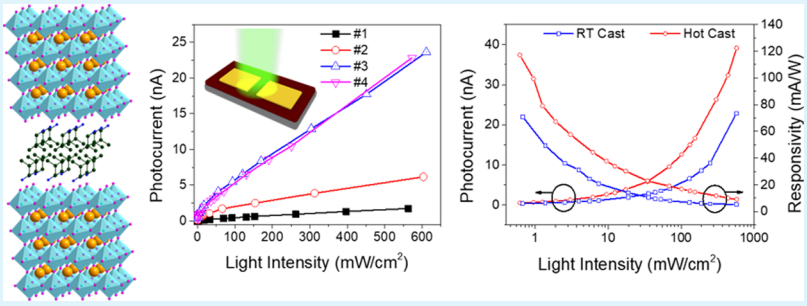

ABSTRACT: Quasi two-dimensional (2D) layered organic−inorganic perovskite materials (e.g., $(BA)_2(MA)_{n-1}Pb_nI_{3n+1}$; BA = butylamine; MA = methylamine) have recently attracted wide attention because of their superior moisture stability as compared with three-dimensional counterparts. Inevitably, hydrophobic yet insulating long-chained organic cations improve the stability at the cost of hindering charge transport, leading to the unsatisfied performance of subsequently fabricated devices. Here, we reported the synthesis of quasi-2D $(iBA)_2(MA)_{n-1}Pb_nI_{3n+1}$ perovskites, where the relatively pure-phase $(iBA)_2PbI_4$ and $(iBA)_2MA_3Pb_4I_{13}$ films can be obtained. Because of the shorter-branched chain of *i*BA as compared with that of its linear equivalent (*n*-butylamine, BA), the resulting $(iBA)_2(MA)_{n-1}Pb_nI_{3n+1}$ perovskites exhibit much enhanced photodetection properties without sacrificing their excellent stability. Through hot-casting, the optimized $(iBA)_2(MA)_{n-1}Pb_nI_{3n+1}$ perovskite films with $n = 4$ give the significantly improved crystallinity, demonstrating the high responsivity of 117.09 mA/W, large on−off ratio of 4.0×10^2, and fast response speed (rise and decay time of 16 and 15 ms, respectively). These figure-of-merits are comparable or even better than those of state-of-the-art quasi-2D perovskite-based photodetectors reported to date. Our work not only paves a practical way for future perovskite photodetector fabrication via modulation of their intrinsic material properties but also provides a direction for further performance enhancement of other perovskite optoelectronics.

KEYWORDS: *quasi-2D, Ruddlesden−Popper perovskite, thin film, short-chained spacer, hot-cast, photodetection*

INTRODUCTION

In recent years, three-dimensional (3D) organic−inorganic halide perovskite materials, such as $MAPbI_3$ ($MA = CH_3NH_3^+$), have attracted wide attention because of the fast development of solar cells based on them.[1−4] Particularly, the power conversion efficiency of these 3D hybrid halide perovskites has been increased from 3.81 to 22.1% in just a few years.[5−8] Owing to the excellent light absorption coefficients, long charge diffusion lengths, high carrier mobility, direct band gap, and low rates of nonradiative charge recombination,[9,10] organic−inorganic halide perovskites also find extensive applications in light-emitting diodes (LEDs),[11−13] photodetectors (PDs),[14,15] nanolasers,[16] transistors,[17] etc. However, these perovskite materials still inevitably suffer from the inherent instability over moisture, heat, and light, which seriously hampers their practical utilizations.[18,19]

At the same time, quasi two-dimensional (quasi-2D) layered perovskite materials (also known as Ruddlesden−Popper, RP, phases) have the crystal structure consisting of quasi-2D perovskite slabs interleaved with cations,[20] in which they generally adopt a chemical formula of $L_2A_{n-1}B_nX_{3n+1}$, where L is a large size or long-chain organic cation, A is a regular cation, B is a divalent metal cation, and X is a halide.[21−23] The variable *n* is an integer, indicating the number of metal halide octahedral

Received: March 1, 2018
Accepted: May 9, 2018
Published: May 9, 2018

DOI: 10.1021/acsami.8b03517
ACS Appl. Mater. Interfaces 2018, 10, 19019−19026

layers between the two L cation layers.[24−26] For example, for $(BA)_2(MA)_{n-1}Pb_nI_{3n+1}$ (BA = $CH_3(CH_2)_3NH_3^+$, MA = $CH_3NH_3^+$) materials, the $(MA)_{n-1}Pb_nI_{3n+1}$ layer is sandwiched by two BA layers. These basic layers would then stack along the *c* axis via van der Waals interaction, forming the bulk quasi-2D layered perovskite material. If *n* becomes infinite, the material would become $MAPbI_3$, the conventional 3D perovskite material. Lately, it has been reported that these quasi-2D layered perovskite materials are more stable as compared with their 3D counterparts.[27,28] Smith et al. demonstrated that $(PEA)_2(MA)_2Pb_3I_{10}$ (PEA = $C_6H_5(CH_2)_2NH_3^+$) can be simply deposited by spin-coating and subsequent high-temperature annealing processes as high-quality quasi-2D layered perovskite films with the good moisture stability, where the fabricated perovskite solar cells exhibit a power conversion efficiency of 4.73%.[29] In addition, Cao et al. also prepared a series of $(BA)_2(MA)_{n-1}Pb_nI_{3n+1}$ with *n* = 1, 2, 3, 4 and found that these quasi-2D perovskites are surprisingly stable, in which the correspondingly fabricated solar cells can retain their photovoltaic performance even after long-duration exposure in humidity environments.[30] Thereafter, the widespread investigation on exploring the fundamental properties of quasi-2D perovskites and their exploitations in high-performance optoelectronic devices have been stimulated. Guo and his group thoroughly studied the electron-phonon scattering of atomically thin $(BA)_2(MA)_{n-1}Pb_nI_{3n+1}$ layers,[31] while Kamminga et al. systematically investigated the quantum confinement phenomena in these low-dimensional lead iodide perovskite hybrids.[32] Dou and his team also prepared $(BA)_2PbBr_4$ flakes with the atomic thickness and revealed their thickness-dependent photoluminescence (PL), being similar to the graphene-like 2D materials.[33] Notably, Liang et al. fabricated LEDs based on $(PEA)_2PbBr_4$ (PEA = $C_6H_5CH_2CH_2NH_3^+$), which yield the efficient room-temperature violet electroluminescence at 410 nm with a narrow bandwidth.[47] All these findings evidently indicate their great potentials as the active materials in state-of-the-art optoelectronics.

Among many quasi-2D layered perovskite materials, $(BA)_2(MA)_{n-1}Pb_nI_{3n+1}$ is one of the most intensively studied materials because of the ease of its synthesis and unique properties. Interestingly, the fabricated film of $(BA)_2(MA)_{n-1}Pb_nI_{3n+1}$ is shown with the *n*-dependent orientation. When *n* is below 4, the film maintains a preferential orientation of the basal plane (i.e., the sandwiched plane). For *n* = 4, the film does not display any more the basal plane orientation. In this case, because the BA layer is insulating, being detrimental for the carrier transport, the resulting film would yield the poor photoelectric properties.[34] Taking it into consideration, Tsai et al. have made use of this character and optimized to obtain $(BA)_2(MA)_3Pb_4I_{13}$-based solar cells, which exhibit the much enhanced photovoltaic efficiency of 12.5%.[27] Inevitably, as the large BA spacer cation possesses the long linear chain hindering the collection of charge carriers, the corresponding carrier mobility would get degraded, particularly in the deep layer of the perovskites, and hence significantly undermine their optoelectronic performances. It is noted that when the linear chain BA cation is substituted by the branched chain *i*BA counterpart, the obtained film crystallinity as well as the air stability would get improved, which can be attributed to the more effective packing of branched alkane chains.[35] The solar cells based on hot-casted $(iBA)_2(MA)_3Pb_4I_{13}$ films can then yield a respectable power conversion efficiency of 10.63%.[35] In any case, there is still very limited investigation on the systematic synthesis and the effect of crystal orientation on the optoelectronic properties of $(iBA)_2(MA)_{n-1}Pb_nI_{3n+1}$ layered perovskites with varied values of *n*.

In this work, iso-butylamine (*i*BA), an isomer to linear *n*-butylamine (BA), has short-branched chain and is deliberately chosen as the spacer cation to synthesize a set of novel quasi-2D RP perovskites. In specific, we have systematically investigated the synthesis of $(iBA)_2(MA)_{n-1}Pb_nI_{3n+1}$ (*n* = 1, 2, 3, and 4) layered perovskite films and found that relatively pure phases can be obtained for *n* = 1 and 4. Mixed phases are obtained for *n* = 2 and 3 with the main phase of $(iBA)_2PbI_4$ and $(iBA)_2MAPb_2I_7$, respectively. All these films exhibit the excellent stability in air, without any noticeable degradation even after the exposure in controlled humidity environments for 60 days. Importantly, PDs made from these layered perovskite films are demonstrated with the impressive photosensing performance. Through a hot-casting method, the 2D perovskite with *n* = 4, namely, $(iBA)_2(MA)_3Pb_4I_{13}$, reveals the improved crystallinity and the PD performance, which are comparable with or even better than those of state-of-the-art quasi-2D perovskite PDs reported to date. All these results not only provide important guidelines for the future quasi-2D RP perovskite-based device construction from the viewpoint of tailoring intrinsic material properties via their synthesis but also offer a direction for the further performance enhancement of other quasi-2D perovskite optoelectronic devices.

EXPERIMENTAL SECTION

Perovskite Precursor Synthesis. Precursor solutions were prepared by dissolving PbI_2, $C_4H_9NH_2$, HI, and CH_3NH_3I at a molar ratio of *n*:2:2:*n* − 1 in dimethyl formamide (DMF). The total Pb^{2+} molar concentration is 2 M in the solutions. The solutions were then stirred at room temperature overnight.

Device Fabrication. The fabrication of PDs started with the one-step spin-coating method of perovskite precursor solution in a nitrogen-filled glovebox, where the oxygen and moisture concentration are well-controlled at the ppm level. Specifically, the glass substrates were first ultrasonically washed by acetone and ethanol and deionized water for 15 min in succession, followed by a mild oxygen plasma treatment for 5 min (0.26 Torr, 30 W). After that, 50 μL of precursor solution was spin-coated on the glass substrate at 3000 rpm for 30 s, subsequently with a thermal annealing at 100 °C for 15 min for the full crystallization of samples. The samples for *n* = 1, 2, 3, and 4 are labeled as #1, #2, #3, and #4, respectively. The thickness of the samples was determined by atomic force microscopy (AFM) and is found to be 665, 405, 540, and 419 nm for #1, #2, #3, and #4, respectively. In the case of employing hot-casting during the fabrication, prior to spin-coating, the precursor solution and substrate were preheated at 120 °C. Then, the hot-casted sample #4 has a thickness of 529 nm. Finally, with the assistance of a shadow mask, gold (100 nm) was thermally evaporated on the films as electrodes. The channel length of the devices is 10 μm.

Film and Device Characterization. Surface morphologies of all the samples were characterized with scanning electron microscopy (SEM, Quanta FEG450) and AFM (diMultimode V, Veeco). X-ray diffraction (XRD, D2 PHASER with Cu Kα radiation, Bruker) was used to evaluate the crystallinity and crystal structure of the products. UV−vis absorption spectra were recorded using a PerkinElmer model Lambda 2S UV−vis spectrometer. The PL spectra were acquired by iHR320 photoluminescence spectroscopy with an excitation wavelength of 425 nm. Time-resolved photoluminescence (TRPL) measurement was performed on a time-correlated single-photon counting spectrometer from Edinburgh Instruments (LifeSpec II). The electrical performance of the fabricated device was characterized with a standard electrical probe station and an Agilent 4155C semiconductor analyzer (Agilent Technologies, California, USA). A 532 nm laser diode was used as the light source for the photodetection

DOI: 10.1021/acsami.8b03517
ACS Appl. Mater. Interfaces 2018, 10, 19019−19026

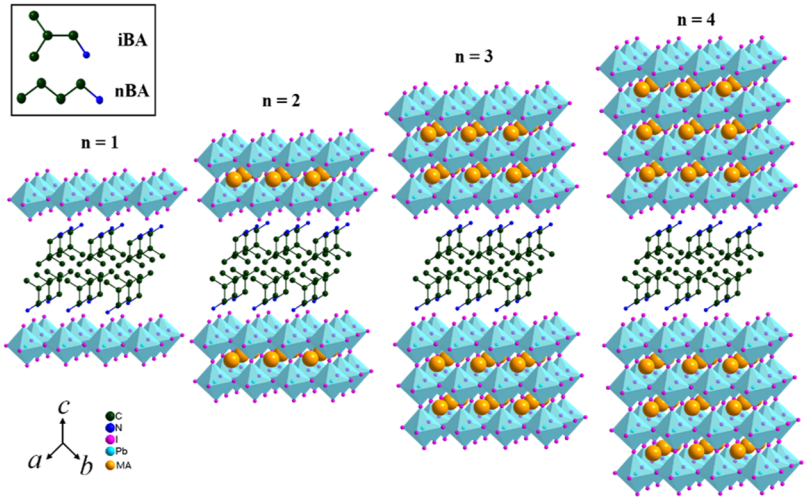

Figure 1. Schematic illustration of the crystal structure of layered perovskite materials with chemical formula $(i\mathrm{BA})_2(\mathrm{MA})_{n-1}\mathrm{Pb}_n\mathrm{I}_{3n+1}$ (n = 1, 2, 3, and 4). Inset shows the chemical structures of *i*BA and *n*BA. All hydrogen atoms are omitted.

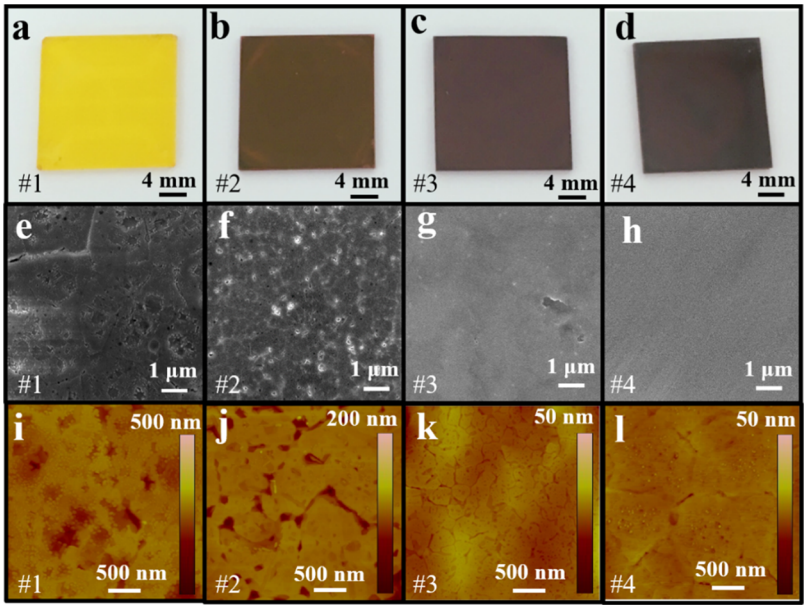

Figure 2. Characterization of the surface morphology of fabricated samples. (a–d) Optical images. (e–h) SEM images. (i–l) AFM images.

measurement, while the power of the incident irradiation was measured using a power meter (PM400, Thorlabs). An attenuator was also employed to tune the irradiation power that was illuminated on the device. For determining the response time of the PD, a low-noise current amplifier (SR570, Stanford Research Systems, USA) combined with a digital oscillator (TBS 1102B EDU, Tektronix, USA) was used to obtain high-resolution current–time curves.

RESULTS AND DISCUSSION

In general, the crystal structure of $(i\mathrm{BA})_2(\mathrm{MA})_{n-1}\mathrm{Pb}_n\mathrm{I}_{3n+1}$ is similar to that of $(\mathrm{BA})_2(\mathrm{MA})_{n-1}\mathrm{Pb}_n\mathrm{I}_{3n+1}$, which also has the layered structure. As shown in Figure 1, the $(\mathrm{MA})_{n-1}\mathrm{Pb}_n\mathrm{I}_{3n+1}$ layer is sandwiched by *i*BA organic layers with the branched chain. The branched chain of *i*BA has been shown to improve the corresponding stability of fabricated perovskite films as compared with those of straight chain BA-sandwiched layers with the exact enhancement mechanism remained uncertain. Anyhow, in the chemical formula, n represents the layer number of the PbI_6 octahedral stacked along c axis. In order to obtain the layered perovskite with predefined n, the precursor solutions can be prepared to consist of PbI_2, $\mathrm{C}_4\mathrm{H}_9\mathrm{NH}_2$, HI, and $\mathrm{CH}_3\mathrm{NH}_3\mathrm{I}$ at a specific stoichiometric ratio of n:2:2:n − 1 (n = 1, 2, 3, and 4) in DMF. The samples with different ratio are then labeled as #1, #2, #3, and #4 for n = 1, 2, 3, and 4, respectively. As depicted in the optical images of all the samples (Figure 2a–d), changes in the stoichiometric ratio are indeed observed to have a profound effect on the resulting films. When n is increased from 1 to 4, the color of the perovskite films gradually varies from yellow to brownish black. To obtain further insights into the difference in their morphologies, SEM and AFM are carried out, accordingly (Figure 2e–i). Obviously, when n is 1, the film shows a rough surface with the presence of pinholes with the size of hundred nanometers, which is known to be detrimental to the interfacial interaction and leads to the significant current leakage for subsequent device fabrication. In contrast, when n is increased to 2, the film starts to become more uniform, although the pinholes can still be clearly observed. Further increasing n to 3 and 4, the films are featured

DOI: 10.1021/acsami.8b03517
ACS Appl. Mater. Interfaces 2018, 10, 19019–19026

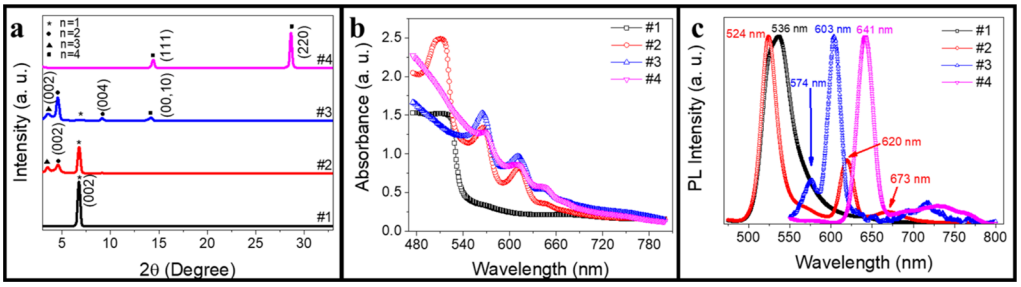

Figure 3. XRD and optical spectra characterization of the samples. (a) XRD patterns. (b) Absorption spectra. (c) PL spectra with an excitation wavelength of 425 nm.

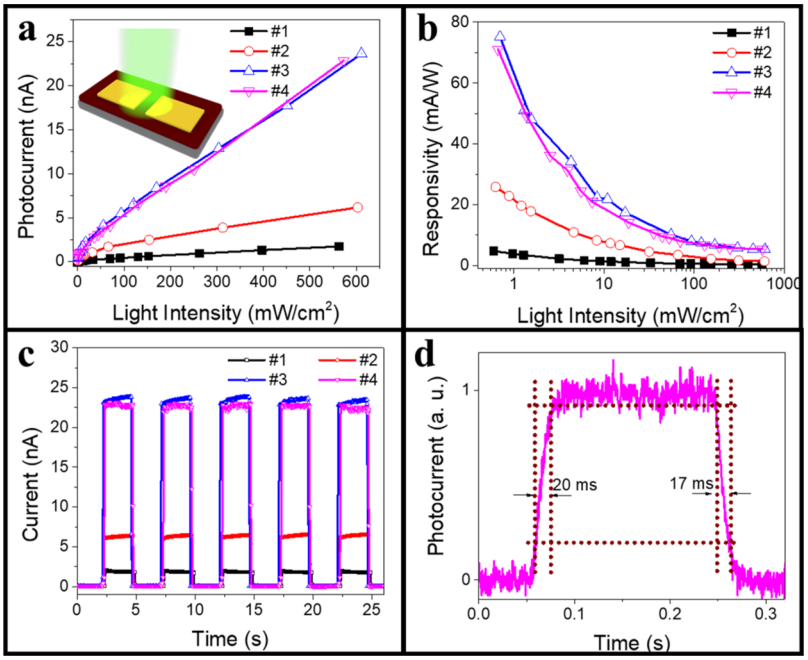

Figure 4. Photoresponse properties of the configured devices. (a) Photocurrent vs light intensity. Inset: schematic illustration of the PD device structure. (b) Responsivity vs light intensity. (c) Current vs time under modulated incident light. (d) High-resolution current vs time curve for sample #4. For (b–d), the bias voltage is 1.5 V. The incident light wavelength is 532 nm. The light intensity for (c,d) is 0.6 W/cm^2.

with the full film coverage without any observable pinholes, simultaneously with the satisfied film uniformity. The morphology change may be due to preferential out-of-plane crystal orientation with the increasing value of n,[46] which will be discussed in detail below. Also, as well-reported in the literature, perovskites with the full film coverage are beneficial as the active sensing materials for high-performance PDs; therefore, it is highly predicted that the perovskite films with n = 3 and 4 are of great potential in fabricating the high-performance optoelectronic devices.

To shed light evaluating the crystal structure of fabricated quasi-2D perovskite films, XRD patterns are acquired as shown in Figure 3a. It is observed that for sample #1, there is merely a pronounced peak located at 6.7°, corresponding to the (002) facet of $(iBA)_2PbI_4$. This indicates that without the MA^+ inclusion, the perovskite film is a pure phase of $(iBA)_2PbI_4$, which has a preferential orientation along c-axis. When the nominal stoichiometric formula changes to n = 2 (sample #2), in addition to the peak of (002) from $(iBA)_2PbI_4$, two tiny diffraction peaks at 3.5° and 4.6° appear, which are attributed to the (002) facets of $(iBA)_2MAPb_2I_7$ and $(iBA)_2(MA)_2Pb_3I_{10}$, respectively.[36,37] This suggests that the main phase of sample #2 is $(iBA)_2PbI_4$ with a small amount of $(iBA)_2MAPb_2I_7$ and $(iBA)_2(MA)_2Pb_3I_{10}$. When the nominal stoichiometric formula varies to n = 3 (sample #3), the main phase becomes $(iBA)_2MAPb_2I_7$ there as validated by the dominant (002) peak of $(iBA)_2MAPb_2I_7$. Regardless, a small amount of $(iBA)_2PbI_4$, $(iBA)_2MA_2Pb_3I_{10}$, and $(iBA)_2MA_3Pb_4I_{13}$ still exists in sample #3. Interestingly, further changing the nominal stoichiometric formula to n = 4, only the (111) and (220) peaks corresponding to $(iBA)_2MA_3Pb_4I_{13}$ are observed, designating sample #4 is a relatively pure phase of $(iBA)_2MA_3Pb_4I_{13}$ with chemical composition equal to the stoichiometry of the precursors. All these observations indicate the complex chemical reactions performed in the solution and nucleations during the film formation.

Apart from the crystal structure, the absorption spectra of all the films are also obtained and shown in Figure 3b. For sample #1, only one absorption edge near 532 nm is observed, suggesting the pure phase of the sample with a band gap of 2.33 eV. For sample #4, three absorption peaks are observed, which are consistent with the previous report[35] with the peaks originated from excitonic absorptions. As samples #2 and #3 are mixed phases, the absorption spectra include multiple absorption peaks, which are in perfect agreements with the XRD results. Notably, all the samples display the absorption

DOI: 10.1021/acsami.8b03517
ACS Appl. Mater. Interfaces 2018, 10, 19019–19026

tails, which are probably contributed from the small impurities of intergrown higher-order homologous members. PL spectra of the samples are also shown in Figure 3c. Sample #1 shows a single emission peak centered at 536 nm, similar to the one of $(BA)_2PbI_4$,[25] demonstrating again sample #1 being the pure-phase $(iBA)_2PbI_4$. For sample #4, there is a prominent emission peak centered at 641 nm, which might be ascribed to the excitonic emission from $(iBA)_2(MA)_3Pb_4I_{13}$, similar to the observation of PL spectrum of $(BA)_2(MA)_3Pb_4I_{13}$.[25] It is shown that only trace amounts of $n = \infty$ phase can be observed from the PL spectrum, and they are even not visible in the XRD pattern of the #4 film. In this case, we anticipate that the as-synthesized $n = 4$ perovskite film is relatively pure with only small inclusions of impurity phases. Also, multiple emission peaks are observed for samples #2 and #3. The prominent emission peak centered at 524 nm for sample #2 can be assigned to $(iBA)_2PbI_4$, although it shows a slight blue shift, whereas the dominant peak centered at 627 nm for sample #3 might be ascribed to $(iBA)_2MAPb_2I_7$ because the main phase of sample #3 is $(iBA)_2MAPb_2I_7$. The second peak centered at 620 nm for sample #2 may be attributed to $(iBA)_2MAPb_2I_7$ because it is close to the dominant peak of sample #3. Further investigations are needed for assessing the origin of other observed peaks.

At the same time, because the ambient stability of quasi-2D perovskites is essential for their practical utilizations, the stability of fabricated $(iBA)_2(MA)_{n-1}Pb_nI_{3n+1}$ films is thoroughly evaluated by storing them under the relative humidity of 50% for 60 days. From the optical image of all the samples, there is not any obvious change observed in the film color (Figure S1 insets). For further demonstration, XRD patterns of the fresh and aged $(iBA)_2(MA)_{n-1}Pb_nI_{3n+1}$ films are measured and shown in Figure S1. Because there is not any noticeable change witnessed from the XRD patterns, the good stability of the quasi-2D layered perovskite films is inferred in humidity environments. To compare the ambient stability of $MAPbI_3$ and quasi-2D $(iBA)_2(MA)_{n-1}Pb_nI_{3n+1}$, $MAPbI_3$ thin films were also prepared and stored under the same humidity. It is observed that the $MAPbI_3$ film gets degraded in a few days as the degradation can be obviously seen from the XRD patterns and optical photographs as shown in Figure S2. Explicitly, the inner side, especially the MA^+, is protected by the encapsulating *i*BA layer, which leads to the good stability as compared with $MAPbI_3$. The impressive air stability of all the quasi-2D layered perovskite films would make them suitable for various technological applications.

In order to assess the photosensing performance of synthesized quasi-2D layered perovskite films, PDs based on the simple two-electrode configuration are fabricated with the device shown in Figure 4a inset. As shown in Figure S3, the current−voltage (I−V) curves of the representative perovskite PDs are measured in the dark and under 532 nm light illumination with different power densities. The devices exhibit the output current as low as approximately 1.3×10^{-11} to 3.1×10^{-9} A at the voltage bias of 1.5 V in the dark, whereas under light illumination, the current displays a remarkable enhancement with the further increase with the increasing incident light intensities, which indicates the typical light-sensitive properties of the layered perovskite films. Moreover, the I−V curves present the linear dependence on the applied bias for all devices, suggesting the nearly Ohmic contact between thin films and gold electrodes, which is beneficial for the collection of photogenerated carriers. In principle, the photocurrent is always defined as the current difference between dark state and light illumination. To better understand the photosensing characteristics of these 2D perovskites, the dependence of their photocurrent on light intensities is measured and shown in Figure 4a. The measured data can be well-fitted by the following formula

$$I_p = A\Phi^{\beta} \tag{1}$$

where I_p is the photocurrent, A and β are the fitting parameters, and Φ is the light intensity. The parameter of β is determined as 0.76, 0.60, 0.76, and 0.81 for samples #1, #2, #3, and #4, respectively. The sublinear relationship between the photocurrent and light intensity is often observed in layered material-based PDs[38] because of the complex processes of electron−hole generation, trapping, and recombination in the semiconductors.[39] Photoresponsivity (R) is another important parameter to determine the sensitivity of PDs, which is defined as

$$R = \frac{I_p}{\Phi S} \tag{2}$$

where S is the active area of the PD. Next, the photoresponsivity as a function of light intensity is shown in Figure 4b. Because of the sublinear relation of I_p−Φ, the photoresponsivity is kept increasing until the lowest-achievable light intensity reaches 4.78, 25.81, 75.20, and 71.11 mA/W for samples #1, #2, #3, and #4, respectively. These optoelectronic parameters are much higher than those of $(BA)_2(MA)_{n-1}Pb_nI_{3n+1}$-based thin film PDs (3.00, 7.31, and 12.78 mA/W for $n = 1$−3, correspondingly),[34] demonstrating that the substitution of linear BA with branched *i*BA is beneficial for the enhancement of their photosensing performances. Furthermore, the responsivity spectrum of sample #4 (Figure S4) agrees very well with the absorption spectrum (Figure 3b), indicating the good quality of the film. We also notice that the responsivities are much lower than the previously reported in-plane photoconductors based on 3D perovskite films.[15] This relatively low photoresponsivity of the quasi-2D perovskites, as compared with bulk $MAPbI_3$, may be caused by the large exciton binding energy, poor carrier transport along the stacking direction, and poor contact between the 2D perovskites and the electrodes. The electrons and holes are therefore difficult to be separated and collected, which should be the major factor in restricting the photoresponsivity.[37]

Furthermore, current−time (I−t) curves under modulated light are also carefully measured to examine the repeatability of fabricated PDs (Figure 4c). It is found that all the PDs possess effective optical switching behaviors with the good repeatability and respectable on/off ratios of 0.5×10^2, 4.5×10^2, 6.2×10^2, and 4.1×10^2 (532 nm laser, 0.6 W/cm^2) for samples #1, #2, #3, and #4, respectively. Similarly, the response time of the PDs can be extracted from the high-resolution I−t curves as recorded in Figures 4d and S5. The rise and decay time of the device are usually defined as the time taken for the current increase from 10 to 90% of steady-state photocurrent and vice versa, accordingly. It is observed that the rise/decay time is determined to be 49/61, 62/52, 22/18, and 20/17 ms for samples #1, #2, #3, and #4, correspondingly. All these results illustrate clearly that the obtained $(iBA)_2(MA)_{n-1}Pb_nI_{3n+1}$ layered perovskite-based PDs achieve the impressive performance with decent responsivities and superior response speeds.

DOI: 10.1021/acsami.8b03517
ACS Appl. Mater. Interfaces 2018, 10, 19019−19026

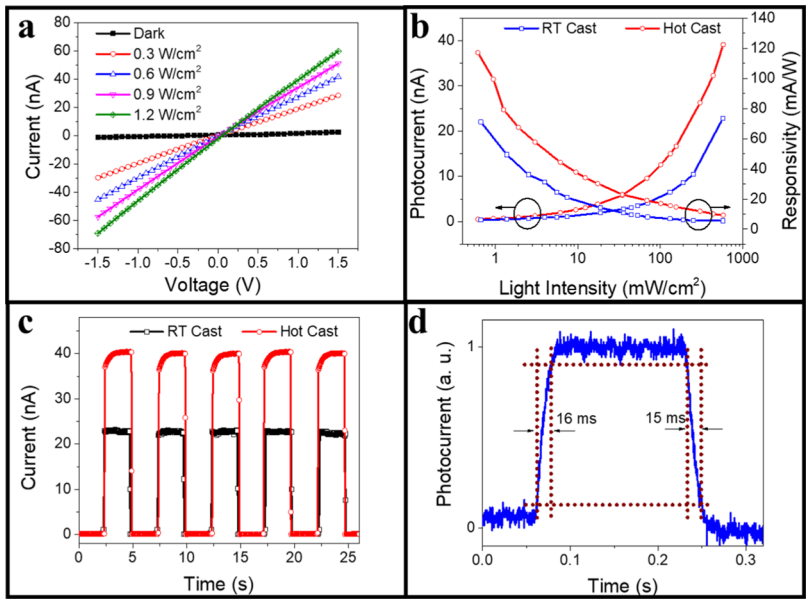

Figure 5. Photoresponse properties of the room-temperature and hot-cast-fabricated samples with the chemical formula $(i\text{BA})_2(\text{MA})_3\text{Pb}_4\text{I}_{13}$. (a) $I-V$ curves with and without light illumination. (b) Photocurrent and responsivity vs light intensity. (c) Current vs time under modulated incident light. (d) High-resolution current vs time curve. For (b–d), the bias voltage is 1.5 V. The incident light wavelength is 532 nm. For (c,d), the light intensity is 0.6 W/cm^2.

As widely reported in the literature, the hot-casting technique can induce the more rapid solvent removal and the higher perovskite crystallization rate during the synthesis of quasi-2D perovskites, which would then lead to the near-single-crystalline orientation and hence the improved charge transport of the fabricated films.[27,30,40,41] Here, because the relatively pure phase as well as the satisfied morphology of $(i\text{BA})_2(\text{MA})_{n-1}\text{Pb}_n\text{I}_{3n+1}$ with $n = 4$ can be easily obtained, the hot-casting method is applied to synthesize the enhanced $(i\text{BA})_2(\text{MA})_3\text{Pb}_4\text{I}_{13}$ films. As anticipated, the sample obtained by hot-casting is demonstrated with the improved diffraction peaks with the same film thickness as compared with the ones without hot-casting, suggesting the better crystallinity (Figure S6). SEM and AFM images indicate that both the room-temperature and hot-cast-fabricated $(i\text{BA})_2(\text{MA})_3\text{Pb}_4\text{I}_{13}$ perovskites are highly smooth and uniform (Figure S7). In particular, well-defined nanoparticles with the high packing density can be observed from the AFM image of the hot-casted $(i\text{BA})_2(\text{MA})_3\text{Pb}_4\text{I}_{13}$ film. Also, TRPL is conducted to investigate the recombination dynamics of the perovskites prepared with and without hot-casting (Figure S8). The total lifetime is found to increase from 4.05 to 6.38 ns after applying hot-casting, further confirming the higher crystal quality of perovskites prepared by the hot-casting method. In view of all these results, we speculate that the hot-cast-fabricated $(i\text{BA})_2(\text{MA})_3\text{Pb}_4\text{I}_{13}$ perovskite is ideal for facilitating the improved performance of optoelectronic devices.

To validate the above hypothesis, the photoresponse measurements of the PDs based on $(i\text{BA})_2(\text{MA})_3\text{Pb}_4\text{I}_{13}$ prepared with and without hot-casting are performed as shown in Figure 5. As shown in the $I-V$ curves of a representative device (Figure 5a), the current is observed to increase with the incident power accordingly, which shows a typical linear relationship with the bias voltage, indicating an Ohmic contact there and thus benefiting the collection of photogenerated carriers. Also, Figure 5b shows the photocurrent and responsivity against the incident light power density. Importantly, the β value is determined to be 0.61 for hot-casted $(i\text{BA})_2(\text{MA})_3\text{Pb}_4\text{I}_{13}$, exhibiting the sublinear relationship between the photocurrent and the incident power density. The photoresponsivity (R), corresponding to the photocurrent spectra, is observed to be a decreasing function of the light intensity, whereas the values of hot-casted perovskite are higher across the entire measured range with the maximum R of 117.09 mA/W. In the photoswitching measurement (Figure 5c), the hot-casted PD displays the current on/off ratio of 4.0×10^2 under a relatively small bias of 1.5 V, and the photocurrent remains almost unchanged after the long duration of switching cycles, indicating its excellent stability and reproducible characteristics. In addition, the rise and decay time constants of hot-casted $(i\text{BA})_2(\text{MA})_3\text{Pb}_4\text{I}_{13}$ device can also be determined from Figure 5d, which is 16 and 15 ms, respectively, showing the faster photoresponse characteristics attributable to its enhanced crystallinity that contributes to the more efficient charge carrier transport and extraction. Specifically, under light illumination, electron–hole pairs are generated and then separated by external electrical field. These electrons and holes would next be collected by the electrodes, separately. During the transport of photogenerated carriers, the carriers would also be trapped by different types of electronic states (e.g., surface traps) or recombined with each other. Here, the high quality of quasi-2D perovskites can ensure the low density of traps and recombination centers, which leads to a longer carrier lifetime. Thus, the quasi-2D perovskite PDs demonstrate the impressive photodetection performance, especially for the hot-casted film with the high crystal quality. It is also noted that all these obtained performance indicators are superior, being comparable with or even better than those of state-of-the-art quasi-2D layered perovskite materials as reported in the recent literatures (Table S1).[21,34,37,42−45] It indicates that our quasi-2D hot-cast-fabricated $(i\text{BA})_2(\text{MA})_3\text{Pb}_4\text{I}_{13}$ perovskite device has the excellent photoresponsivity and fast response time for light detection as well as the promising prospect for high-performance PD applications.

DOI: 10.1021/acsami.8b03517
ACS Appl. Mater. Interfaces 2018, 10, 19019−19026

In addition, the further optimization of $(iBA)_2(MA)_3Pb_4I_{13}$ films shows that the hot-casting method is beneficial for the improvement of PDs judging on the overall performance, which will provide effective modulations over quasi-2D perovskites for utilizations in various optoelectronic switches and PDs.

CONCLUSION

In summary, high-quality $(iBA)_2(MA)_{n-1}Pb_nI_{3n+1}$ layered perovskite films were prepared by the simple spin-coating method, where the relatively pure-phase $(iBA)_2PbI_4$ and $(iBA)_2(MA)_3Pb_4I_{13}$ films can be readily obtained. Importantly, these quasi-2D perovskite films exhibit the impressive photodetection performance, such as the fast response times, low dark current, and decent responsivity. Through the hot-casting method, significant enhancement in the crystallinity can also be achieved for $(iBA)_2(MA)_3Pb_4I_{13}$ perovskite films, which demonstrates the higher responsivity of 117.09 mA/W, larger on−off ratio of 4.0×10^2, and faster response speeds (rise and decay time of 16 and 15 ms, respectively). All these performance parameters are comparable with or even superior to the ones fabricated with the state-of-the-art quasi-2D layered perovskites, highlighting their technological potency of various practical utilizations in optoelectronics. Our work does not only pave a practical way for future quasi-2D perovskite-based PD fabrication via the modulation of its intrinsic material properties but also provides a new road map for future studies in designing and optimizing layered perovskite-based PDs.

ASSOCIATED CONTENT

Supporting Information

The Supporting Information is available free of charge on the ACS Publications website at DOI: 10.1021/acsami.8b03517.

XRD patterns of all the samples showing the stability of quasi-2D layered perovskite films; XRD patterns of $MAPbI_3$ showing the stability of 3D bulk perovskite films; *I*−*V* curves of all the samples with and without light illumination; wavelength-dependent responsivity spectrum of sample #4; high-resolution current versus time under modulated incident light to determine response times; XRD patterns of room temperature and hot-casted $(iBA)_2(MA)_3Pb_4I_{13}$ films; characterization of the morphology of room-temperature and hot-casted $(iBA)_2(MA)_3Pb_4I_{13}$ films; TRPL of room-temperature and hot-casted $(iBA)_2(MA)_3Pb_4I_{13}$ films; and comparison of various figure of merits of different quasi-2D layered perovskite-based PDs (PDF)

AUTHOR INFORMATION

Corresponding Author

*E-mail: johnnyho@cityu.edu.hk.

ORCID

Chun Li: 0000-0002-8190-9843

Johnny C. Ho: 0000-0003-3000-8794

Notes

The authors declare no competing financial interest.

ACKNOWLEDGMENTS

We acknowledge the General Research Fund (CityU 11275961) and the Theme-based Research Scheme (T42-103/16-N) of the Research Grants Council of Hong Kong SAR, China, the National Natural Science Foundation of China (grants 51672229 and 61605024), the Science Technology and Innovation Committee of Shenzhen Municipality (grant JCYJ 20170818095520778), and a grant from the Shenzhen Research Institute, City University of Hong Kong.

REFERENCES

(1) Hodes, G. Perovskite-Based Solar Cells. *Science* **2013**, *342*, 317−318.

(2) He, M.; Pang, X.; Liu, X.; Jiang, B.; He, Y.; Snaith, H.; Lin, Z. Monodisperse Dual-Functional Upconversion Nanoparticles Enabled Near-Infrared Organolead Halide Perovskite Solar Cells. *Angew. Chem., Int. Ed.* **2016**, *55*, 4280−4284.

(3) Shi, S.; Li, Y.; Li, X.; Wang, H. Advancements in All-Solid-State Hybrid Solar Cells Based on Organometal Halide Perovskites. *Mater. Horiz.* **2015**, *2*, 378−405.

(4) He, M.; Zheng, D.; Wang, M.; Lin, C.; Lin, Z. High Efficiency Perovskite Solar Cells: From Complex Nanostructure to Planar Heterojunction. *J. Mater. Chem. A* **2014**, *2*, 5994−6003.

(5) Correa-Baena, J.-P.; Saliba, M.; Buonassisi, T.; Grätzel, M.; Abate, A.; Tress, W.; Hagfeldt, A. Promises and Challenges of Perovskite Solar Cells. *Science* **2017**, *358*, 739−744.

(6) Xu, X.; Ma, C.; Cheng, Y.; Xie, Y.-M.; Yi, X.; Gautam, B.; Chen, S.; Li, H.-W.; Lee, C.-S.; So, F.; Tsang, S.-W. Ultraviolet-Ozone Surface Modification for Non-Wetting Hole Transport Materials Based Inverted Planar Perovskite Solar Cells with Efficiency Exceeding 18%. *J. Power Sources* **2017**, *360*, 157−165.

(7) Yang, W. S.; Park, B.-W.; Jung, E. H.; Jeon, N. J.; Kim, Y. C.; Lee, D. U.; Shin, S. S.; Seo, J.; Kim, E. K.; Noh, J. H. Iodide Management in Formamidinium-Lead-Halide−based Perovskite Layers for Efficient Solar Cells. *Science* **2017**, *356*, 1376−1379.

(8) Kojima, A.; Teshima, K.; Shirai, Y.; Miyasaka, T. Organometal Halide Perovskites as Visible-Light Sensitizers for Photovoltaic Cells. *J. Am. Chem. Soc.* **2009**, *131*, 6050−6051.

(9) Stranks, S. D.; Eperon, G. E.; Grancini, G.; Menelaou, C.; Alcocer, M. J. P.; Leijtens, T.; Herz, L. M.; Petrozza, A.; Snaith, H. J. Electron-Hole Diffusion Lengths Exceeding 1 Micrometer in an Organometal Trihalide Perovskite Absorber. *Science* **2013**, *342*, 341−344.

(10) Burschka, J.; Pellet, N.; Moon, S.-J.; Humphry-Baker, R.; Gao, P.; Nazeeruddin, M. K.; Grätzel, M. Sequential Deposition as a Route to High-Performance Perovskite-Sensitized Solar Cells. *Nature* **2013**, *499*, 316−319.

(11) Bade, S. G. R.; Li, J.; Shan, X.; Ling, Y.; Tian, Y.; Dilbeck, T.; Besara, T.; Geske, T.; Gao, H.; Ma, B. Fully Printed Halide Perovskite Light-Emitting Diodes with Silver Nanowire Electrodes. *ACS Nano* **2015**, *10*, 1795−1801.

(12) Kim, Y.-H.; Cho, H.; Heo, J. H.; Kim, T.-S.; Myoung, N.; Lee, C.-L.; Im, S. H.; Lee, T.-W. Multicolored Organic/Inorganic Hybrid Perovskite Light-Emitting Diodes. *Adv. Mater.* **2015**, *27*, 1248−1254.

(13) Chen, Z.; Zhang, C.; Jiang, X.-F.; Liu, M.; Xia, R.; Shi, T.; Chen, D.; Xue, Q.; Zhao, Y.-J.; Su, S.; et al. High-Performance Color-Tunable Perovskite Light Emitting Devices through Structural Modulation from Bulk to Layered Film. *Adv. Mater.* **2017**, *29*, 1603157.

(14) Dou, L.; Yang, Y.; You, J.; Hong, Z.; Chang, W.-H.; Li, G.; Yang, Y. Solution-Processed Hybrid Perovskite Photodetectors with High Detectivity. *Nat. Commun.* **2014**, *5*, 5404.

(15) Tian, W.; Zhou, H.; Li, L. Hybrid Organic-Inorganic Perovskite Photodetectors. *Small* **2017**, *13*, 1702107.

(16) Fu, Y.; Zhu, H.; Schrader, A. W.; Liang, D.; Ding, Q.; Joshi, P.; Hwang, L.; Zhu, X.-Y.; Jin, S. Nanowire Lasers of Formamidinium Lead Halide Perovskites and Their Stabilized Alloys with Improved Stability. *Nano Lett.* **2016**, *16*, 1000−1008.

(17) Chin, X. Y.; Cortecchia, D.; Yin, J.; Bruno, A.; Soci, C. Lead Iodide Perovskite Light-Emitting Field-Effect Transistor. *Nat. Commun.* **2015**, *6*, 7383.

(18) Wang, Z.; Shi, Z.; Li, T.; Chen, Y.; Huang, W. Stability of Perovskite Solar Cells: A Prospective on the Substitution of the A Cation and X Anion. *Angew. Chem., Int. Ed.* **2017**, *56*, 1190−1212.

(19) Misra, R. K.; Cohen, B.-E.; Iagher, L.; Etgar, L. Low Dimensional Organic-Inorganic Halide Perovskite: Structure, Properties, and Applications. *ChemSusChem* **2017**, *10*, 3712−3721.
(20) Lin, H.; Zhou, C.; Tian, Y.; Siegrist, T.; Ma, B. Low-Dimensional Organometal Halide Perovskites. *ACS Energy Lett.* **2018**, *3*, 54−62.
(21) Chen, J.; Wang, Y.; Gan, L.; He, Y.; Li, H.; Zhai, T. Generalized Self-Doping Engineering towards Ultrathin and Large Sized Two-Dimensional Homologous Perovskite. *Angew. Chem., Int. Ed.* **2017**, *129*, 15089−15093.
(22) Zhang, X.; Wu, G.; Yang, S.; Fu, W.; Zhang, Z.; Chen, C.; Liu, W.; Yan, J.; Yang, W.; Chen, H. Vertically Oriented 2D Layered Perovskite Solar Cells with Enhanced Efficiency and Good Stability. *Small* **2017**, *13*, 1700611.
(23) Cheng, Z.; Lin, J. Layered Organic−inorganic Hybrid Perovskites: Structure, Optical Properties, Film Preparation, Patterning and Templating Engineering. *CrystEngComm* **2010**, *12*, 2646−2662.
(24) Kagan, C. R.; Mitzi, D. B.; Dimitrakopoulos, C. D. Organic-Inorganic Hybrid Materials as Semiconducting Channels in Thin-Film Field-Effect Transistors. *Science* **1999**, *286*, 945−947.
(25) Stoumpos, C. C.; Cao, D. H.; Clark, D. J.; Young, J.; Rondinelli, J. M.; Jang, J. I.; Hupp, J. T.; Kanatzidis, M. G. Ruddlesden-Popper Hybrid Lead Iodide Perovskite 2D Homologous Semiconductors. *Chem. Mater.* **2016**, *28*, 2852−2867.
(26) Yuan, Z.; Shu, Y.; Xin, Y.; Ma, B. Highly Luminescent Nanoscale Quasi-2D Layered Lead Bromide Perovskites with Tunable Emissions. *Chem. Commun.* **2016**, *52*, 3887−3890.
(27) Tsai, H.; Nie, W.; Blancon, J.-C.; Stoumpos, C. C.; Asadpour, R.; Harutyunyan, B.; Neukirch, A. J.; Verduzco, R.; Crochet, J. J.; Tretiak, S.; Pedesseau, L.; Even, J.; Alam, M. A.; Gupta, G.; Lou, J.; Ajayan, P. M.; Bedzyk, M. J.; Kanatzidis, M. G.; Mohite, A. D. High-Efficiency Two-Dimensional Ruddlesden−Popper Perovskite Solar Cells. *Nature* **2016**, *536*, 312−316.
(28) Shang, Q.; Wang, Y.; Zhong, Y.; Mi, Y.; Qin, L.; Zhao, Y.; Qiu, X.; Liu, X.; Zhang, Q. Unveiling Structurally Engineered Carrier Dynamics in Hybrid Quasi-Two-Dimensional Perovskite Thin Films toward Controllable Emission. *J. Phys. Chem. Lett.* **2017**, *8*, 4431−4438.
(29) Smith, I. C.; Hoke, E. T.; Solis-Ibarra, D.; McGehee, M. D.; Karunadasa, H. I. A Layered Hybrid Perovskite Solar-Cell Absorber with Enhanced Moisture Stability. *Angew. Chem., Int. Ed.* **2014**, *53*, 11232−11235.
(30) Cao, D. H.; Stoumpos, C. C.; Farha, O. K.; Hupp, J. T.; Kanatzidis, M. G. 2D Homologous Perovskites as Light-Absorbing Materials for Solar Cell Applications. *J. Am. Chem. Soc.* **2015**, *137*, 7843−7850.
(31) Guo, Z.; Wu, X.; Zhu, T.; Zhu, X.; Huang, L. Electron−phonon Scattering in Atomically Thin 2D Perovskites. *ACS Nano* **2016**, *10*, 9992−9998.
(32) Kamminga, M. E.; Fang, H.-H.; Filip, M. R.; Giustino, F.; Baas, J.; Blake, G. R.; Loi, M. A.; Palstra, T. T. M. Confinement Effects in Low-Dimensional Lead Iodide Perovskite Hybrids. *Chem. Mater.* **2016**, *28*, 4554−4562.
(33) Dou, L.; Wong, A. B.; Yu, Y.; Lai, M.; Kornienko, N.; Eaton, S. W.; Fu, A.; Bischak, C. G.; Ma, J.; Ding, T.; Ginsberg, N. S.; Wang, L.-W.; Alivisatos, A. P.; Yang, P. Atomically Thin Two-Dimensional Organic-Inorganic Hybrid Perovskites. *Science* **2015**, *349*, 1518−1521.
(34) Zhou, J.; Chu, Y.; Huang, J. Photodetectors Based on Two-Dimensional Layer-Structured Hybrid Lead Iodide Perovskite Semiconductors. *ACS Appl. Mater. Interfaces* **2016**, *8*, 25660−25666.
(35) Chen, Y.; Sun, Y.; Peng, J.; Zhang, W.; Su, X.; Zheng, K.; Pullerits, T.; Liang, Z. Tailoring Organic Cation of 2D Air-Stable Organometal Halide Perovskites for Highly Efficient Planar Solar Cells. *Adv. Energy Mater.* **2017**, *7*, 1700162.
(36) Chen, J.; Gan, L.; Zhuge, F.; Li, H.; Song, J.; Zeng, H.; Zhai, T. A Ternary Solvent Method for Large-Sized Two-Dimensional Perovskites. *Angew. Chem., Int. Ed.* **2017**, *56*, 2390−2394.
(37) Yu, D.; Cao, F.; Shen, Y.; Liu, X.; Zhu, Y.; Zeng, H. Dimensionality and Interface Engineering of 2D Homologous Perovskites for Boosted Charge Carrier Transport and Photodetection Performances. *J. Phys. Chem. Lett.* **2017**, *8*, 2565−2572.
(38) Lan, C.; Dong, R.; Zhou, Z.; Shu, L.; Li, D.; Yip, S.; Ho, J. C. Large-Scale Synthesis of Freestanding Layer-Structured PbI_2 and $MAPbI_3$ Nanosheets for High-Performance Photodetection. *Adv. Mater.* **2017**, *29*, 1702759.
(39) Binet, F.; Duboz, J. Y.; Rosencher, E.; Scholz, F.; Härle, V. Mechanisms of Recombination in GaN Photodetectors. *Appl. Phys. Lett.* **1996**, *69*, 1202−1204.
(40) Blancon, J.-C.; Tsai, H.; Nie, W.; Stoumpos, C. C.; Pedesseau, L.; Katan, C.; Kepenekian, M.; Soe, C. M. M.; Appavoo, K.; Sfeir, M. Y. Extremely Efficient Internal Exciton Dissociation through Edge States in Layered 2D Perovskites. *Science* **2017**, *355*, 1288−1292.
(41) Liu, B.; Soe, C. M. M.; Stoumpos, C. C.; Nie, W.; Tsai, H.; Lim, K.; Mohite, A. D.; Kanatzidis, M. G.; Marks, T. J.; Singer, K. D. Optical Properties and Modeling of 2D Perovskite Solar Cells. *Phys. Status Solidi RRL* **2017**, *1*, 1700062.
(42) Li, L.; Sun, Z.; Wang, P.; Hu, W.; Wang, S.; Ji, C.; Hong, M.; Luo, J. Tailored Engineering of an Unusual $(C_4H_9NH_3)_2(CH_3NH_3)_2Pb_3Br_{10}$ Two-Dimensional Multilayered Perovskite Ferroelectric for a High-Performance Photodetector. *Angew. Chem., Int. Ed.* **2017**, *56*, 12150−12154.
(43) Peng, W.; Yin, J.; Ho, K.-T.; Ouellette, O.; De Bastiani, M.; Murali, B.; El Tall, O.; Shen, C.; Miao, X.; Pan, J.; Alarousu, E.; He, J. H.; Ooi, B. S.; Mohammed, O. F.; Sargent, E.; Bakr, O. M. Ultralow Self-Doping in Two-Dimensional Hybrid Perovskite Single Crystals. *Nano Lett.* **2017**, *17*, 4759−4767.
(44) Tan, Z.; Wu, Y.; Hong, H.; Yin, J.; Zhang, J.; Lin, L.; Wang, M.; Sun, X.; Sun, L.; Huang, Y.; Liu, K.; Liu, Z.; Peng, H. Two-Dimensional $(C_4H_9NH_3)_2PbBr_4$ Perovskite Crystals for High-Performance Photodetector. *J. Am. Chem. Soc.* **2016**, *138*, 16612−16615.
(45) Zhu, B.-S.; He, Z.; Yao, J.-S.; Chen, C.; Wang, K.-H.; Yao, H.-B.; Liu, J.-W.; Yu, S.-H. Potassium Ion Assisted Synthesis of Organic-Inorganic Hybrid Perovskite Nanobelts for Stable and Flexible Photodetectors. *Adv. Opt. Mater.* **2017**, *6*, 1701029.
(46) Wang, R.; Tong, Y.; Manzi, A.; Wang, K.; Fu, Z.; Kentzinger, E.; Feldmann, J.; Urban, A. S.; Müller-Buschbaum, P.; Frielinghaus, H. Preferential Orientation of Crystals Induced by Incorporation of Organic Ligands in Mixed-Dimensional Hybrid Perovskite Films. *Adv. Opt. Mater.* **2018**, *6*, 1701311.
(47) Liang, D.; Peng, Y.; Fu, Y.; Shearer, M. J.; Zhang, J.; Zhai, J.; Zhang, Y.; Hamers, R. J.; Andrew, T. L.; Jin, S. Color-Pure Violet-Light-Emitting Diodes Based on Layered Lead Halide Perovskite Nanoplates. *ACS Nano* **2016**, *10*, 6897−6904.

DOI: 10.1021/acsami.8b03517
ACS Appl. Mater. Interfaces 2018, 10, 19019−19026